International Journal of Applied Earth Observations and Geoinformation 109 (2022) 102801

Contents lists available at ScienceDirect

International Journal of Applied Earth Observations and Geoinformation

journal homepage: www.elsevier.com/locate/jag

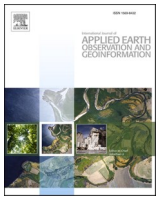

Automated soybean mapping based on canopy water content and chlorophyll content using Sentinel-2 images

Yingze Huang [a], Bingwen Qiu [a,*], Chongcheng Chen [a], Xiaolin Zhu [b], Wenbin Wu [c], Fanchen Jiang [a], Duoduo Lin [a], Yufeng Peng [a]

[a] Key Laboratory of Spatial Data Mining & Information Sharing of the Ministry of Education, National Engineering Research Centre of Geospatial Information Technology, Fuzhou University, Fuzhou, China
[b] Department of Land Surveying and Geo-Informatics, The Hong Kong Polytechnic University, Hong Kong, China
[c] Key Laboratory of Agricultural Remote Sensing (AGRIRS), Ministry of Agriculture and Rural Affairs/Institute of Agricultural Resources and Regional Planning, Chinese Academy of Agricultural Sciences, Beijing, China

ARTICLE INFO

Keywords:
Phenology-based algorithm
Soybean
Sentinel-2
Time-series analysis
Spatiotemporal changes

ABSTRACT

Accurate and timely spatiotemporal distribution information of soybean is vital for sustainable agriculture development. However, it is challenging to establish a phenology-based automated crops mapping algorithm at large spatial domains by simply applying vegetation index temporal profile. This study developed a Phenology-based automatic Soybean mapping algorithm through combined Canopy water and Chlorophyll variations (PSCC). Three phenology-based indices were designed: the ratio of change magnitudes of vegetation index to water stress index during the late growth stage (T1), the mean concentration of chlorophyll during the whole growth period (T2), and the accumulated variations of chlorophyll before and after heading date (T3). Soybean was distinguished by lower T1 and T3 and higher T1 due to higher senescence water loss and chlorophyll content. The PSCC method was validated in Northeast China from 2017 to 2021 and in four states (Missouri, Illinois, Indiana, and Ohio) of the United States (US) in 2020 using Sentinel-2 datasets. Soybean planting areas obtained by PSCC were consistent with the corresponding agricultural statistical area ($R^2 > 0.83$). The soybean maps were evaluated using 5702 reference data, and the overall accuracy and kappa coefficient were 91.99% and 0.8338, respectively. The overall accuracy for soybean mapping was improved by 16.07% compared with using only canopy water variation. The result showed that our method could be applied to large spatial domains and multi-years without retraining. The soybean planting area in Northeast China expanded substantially 25,867 km^2 (by 89.10%) during the period 2015–2020 and decreased slightly 7,535 km^2 (by 13.73%) from 2020 to 2021. Soybean expansion occurred mainly in ever-planted regions. Northeast China contributed about 60% to the national soybean revitalization goal in 2020. This study provided information on the soybean spatiotemporal changes in Northeast China, which was significant for agricultural policymakers to formulate soybean production plans to achieve national soybean revitalization.

1. Introduction

Soybean is one of the most valuable crops and plays an essential role in global food security and sustainable agriculture development. Soybean is a high-protein food source (Rębilas et al., 2020) and is considered a good substitute for animal protein. Moreover, it also belongs to the type of plant function with ecological significance, and its nitrogen fixation contributes 77% of the global agricultural nitrogen budget (Kumar et al., 2017). In addition, crop rotation with soybean is an effective means to increase crop production and achieve sustainable agriculture (Agomoh et al., 2021). As important soybean producers in the world, China and the US have significantly changed in soybean planting areas in recent years. Therefore, accurate and rapid soybean mapping is essential to ensure global food security and environmental sustainability.

Remote sensing provides a powerful data source for timely delivering the spatiotemporal distribution information of crops at the regional scale (Weiss et al., 2020). Multi-temporal images datasets have been

* Corresponding author at: Spatial Information Research Centre of Fujian Province, Yangguang Keji Building, Floor 8th, Xueyuan Road 2, Fuzhou University, Fuzhou 350116, Fujian, China.
E-mail address: qiubingwen@fzu.edu.cn (B. Qiu).

https://doi.org/10.1016/j.jag.2022.102801
Received 7 January 2022; Received in revised form 19 April 2022; Accepted 22 April 2022
Available online 28 April 2022
1569-8432/© 2022 The Author(s). Published by Elsevier B.V. This is an open access article under the CC BY-NC-ND license (http://creativecommons.org/licenses/by-nc-nd/4.0/).

widely used in crop classification in recent years. Generally, machine learning models, such as support vector machine (Zheng et al., 2015), decision trees (Song et al., 2017), and random forest (Tran et al., 2022) were employed to identify crops. Spectral bands and vegetation indexes were used as input features. However, these models relied on a given dataset and reference data. When applied to other years or regions, most models need to recollect reference data to retrain. The need to map cropland or crops quickly, consistently, and repeatedly requires an automated algorithm that can be employed in other years and regions without retraining (Thenkabail et al., 2009). However, automated algorithms usually rely on substantial expert knowledge to analyze the images (Ashourloo et al., 2020). And the difference in spectral signal between crops may be insignificant, or it can be mined only at certain phenological stages (Waldner et al., 2015; Zhong et al., 2014). Phenology-based approaches rely on crop knowledge and emphasize the significance of the spectral signal of key phenology stages for crop mapping. Therefore, phenology-based approaches may be a valuable resource for rapid, consistent, and repetitive crop mapping (Wang et al., 2019).

Phenology-based crop mapping methods applied the unique spectral characteristics of crucial phenological periods. The vegetation indexes reflecting the phenological characteristics of crops, such as the Normalized Difference Vegetation Index (NDVI), were widely employed to identify crops (Qu et al., 2021; Zhong et al., 2011). However, the temporal profiles of vegetation indices may be affected by inter-annual and regional differences (Qiu et al., 2018). Therefore, it is hard to obtain crop distribution at large spatial domains merely by applying vegetation index (Peña and Brenning, 2015). The phenology-based algorithms combining vegetation indices and other spectral features have advantages in crop mapping over large regions (Dong and Xiao, 2016). A series of phenology-based methods have been successfully developed to identify staple crops, such as winter wheat, paddy rice, and maize (Qiu et al., 2017b; Xiao et al., 2005). For example, given the growth characteristics of paddy rice in flooded soil, the paddy rice mapping methods were widely proposed by combining vegetation index and Land Surface Water Index (LSWI) (Qin et al., 2015; Xiao et al., 2005). Recently, several studies applied the unique characteristic of crop canopy during the critical phenological stage to map crops, such as canola (Tian et al., 2022; Zang et al., 2020) and cotton (Wang et al., 2021; Xun et al., 2021). The Canola Index (CI) was proposed to identify canola using spectral reflectance during the flowering period (Ashourloo et al., 2019). These studies showed that unique crop knowledge is critical in exploring the spectral-temporal characteristics of specific crops. However, it is difficult to observe the growth characteristics of dryland crops (such as potato, peanut, and soybean). Therefore, exploring crop knowledge and introducing new spectral indices are essential to improve specific crop mapping.

A majority of existing soybean mapping efforts were implemented using vegetation indices time series in Brazil and the US (da Silva et al., 2017; de Souza et al., 2015; Esquerdo et al., 2011). Recent studies have verified the effectiveness of canopy water content in distinguishing soybeans and maize (Xu et al., 2021; You et al., 2021; Zhong et al., 2016a). The Shortwave Infrared (SWIR) band has been applied to separate soybean and maize (Zhong et al., 2016a). The water index (i.e., Normalized Differential Senescent Vegetation Index, LSWI) correlated with crop moisture content and was also utilized to classify maize and soybean (Cai et al., 2018; Zhong et al., 2014). However, most previous crop mapping methods used MODIS or Landsat data to effectively use time-series features (Jain et al., 2017; Yang et al., 2019). Another freely available time series dataset with better spatial resolution, frequency revisit (5-day), and red-edge bands, the Sentinel-2 images, provide unprecedented opportunities for crop mapping (Jin et al., 2019). The Sentinel-2 spectral band has shown superiority in soybean and maize classification (Ren et al., 2022). The red-edge bands can efficiently characterize crop conditions and assist in crop classification (Sharifi, 2020; Zhang et al., 2020). But, it is also challenging to discriminate crops with similar phenology and spectral reflectance, such as maize and soybean (Zhang et al., 2020). The ability of important pigments indexes in estimating photosynthetic activity was highlighted in recent studies (Wong et al., 2019), which suggests their potential efficiency in assisting crop mapping. The pigments indexes based on the red edges performed well in peanut mapping and have the capability to map other crops (Qiu et al., 2021). However, the performance of pigment indices is not yet known for other crop mappings.

Therefore, this study explored canopy water and chlorophyll content variations based on sentinel-2 images. Then, new spectral-temporal features were suggested for soybean mapping and tested in Northeast China and four US states. The soybean spatial distribution provided data support for analyzing the changes in the soybean planting area. Two goals were proposed in this study: (1) developing a Phenology-based automated Soybean mapping algorithm through combined Canopy water and Chlorophyll variations (PSCC) using Sentinel-2 time-series images; (2) analyzing the spatiotemporal changes in soybean planting area in Northeast China.

2. Materials

2.1. Study area

Northeast China and four US states (Missouri, Illinois, Indiana, and Ohio) were selected as the study area by considering the availability of reference data (Fig. 1). Northeast China is one of China's most dominant agricultural regions (Fig. 1(a)). It includes Heilongjiang, Jilin, and Liaoning Provinces. Single cropping is implemented in Northeast China due to the temperature limit (Qiu et al., 2017a). The primary crops are soybean, maize, paddy rice, sorghum, peanut, potato, and sunflower. According to the national agricultural statistical data, more than half (53%) of national soybean fields were distributed in Northeast China in 2020. The four US states were selected as the second study area (Fig. 1 (b)). This area has various crops, including soybean, maize, sorghum, spring wheat, sunflower, cotton, potato, and peanut. In 2020, the soybean planting area in four US states reached 108,770 km^2, accounting for 31.78% of the US soybean planting area.

2.2. Datasets

2.2.1. Sentinel-2A/B image

Sentinel-2 data has the advantages of finer spatial resolution (10 m, 20 m, and 60 m) and high revisit capability (5 days). Sentinel-2 carries MultiSpectral Instrument (MSI) that provides 13 spectral bands. The top-of-atmosphere reflectance (TOA) data was applied instead of the surface reflectance data. The TOA data has been proved to be efficient in reflecting the spectral differences between different crops (Jin et al., 2019; Wang et al., 2020). All available Level-1C Sentinel-2A/B images were collected from the Google Earth Engine (GEE) platform. There were 9604, 21,614, 22,622, 22,460, and 22,216 Sentinel-2 images over Northeast China from 2017 to 2021, and 13,464 Sentinel-2 images covering four US states in 2020.

2.2.2. Reference data

Reference data consists of 2,837 sites for Northeast China and 5,000 sites for four US states (Table S1). The reference data in Northeast China was collected through field observations in 2018 and 2020. The ground truth sites included 1,090 soybean sites and 1,747 other crop sites (Fig. 1 (a)). The MG858 hand-held GPS receivers recorded the position of the ground truth site. Moreover, at least one picture recording the growth of crops was taken by a digital camera. We randomly selected 1,900 soybean sites and 3,100 other crop sites based on Cropland Data Layer (CDL) for four US states in 2020 (Fig. 1(b)). The CDL is derived from the United States Department of Agriculture, and it provides high overall accuracy of over 95% for soybean (Boryan et al., 2011).

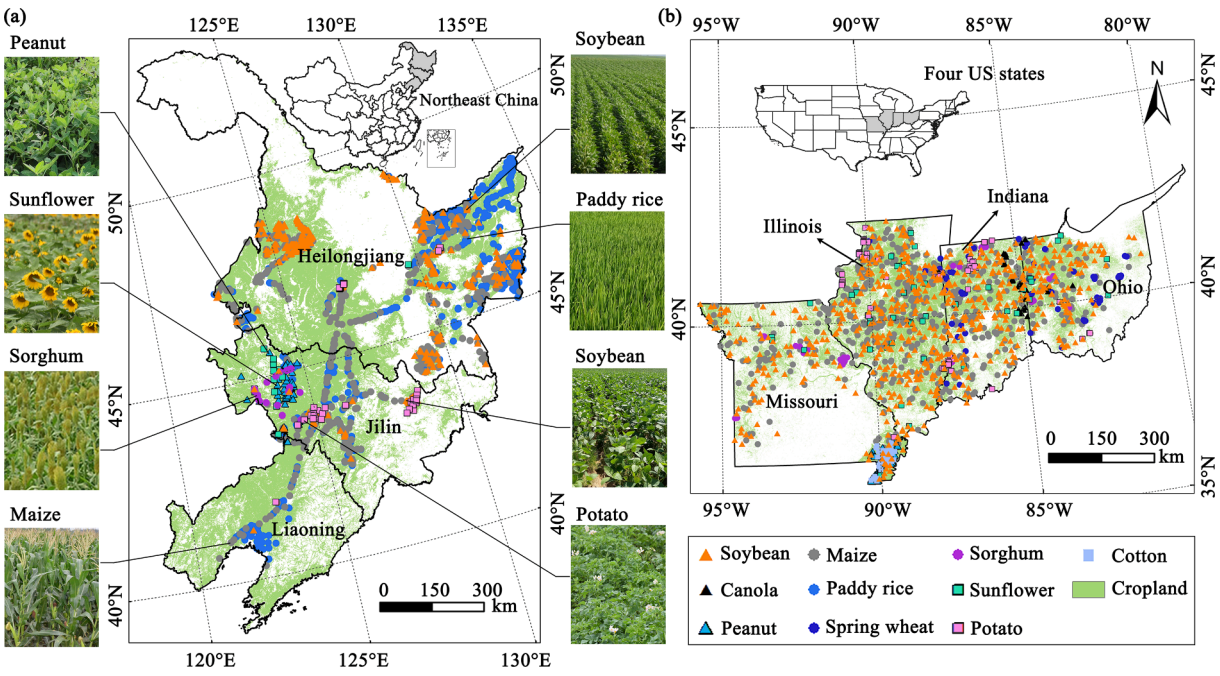

Fig. 1. The location and survey sites of (a) Northeast China and (b) four US states.

2.2.3. Agricultural statistics data, crop calendar data, and cropland data

The provincial statistical yearbooks reported the agricultural statistics data of Heilongjiang, Jilin, and Liaoning Provinces from 2017 to 2019. The agricultural statistics data for four US states were calculated by CDL data in 2020. These statistics data were used to verify Sentinel-2 estimated soybean maps. The changes in soybean planting areas were analyzed by combining the municipal agricultural statistics data of Northeast China in 2008 and 2015.

The crop calendar data of Northeast China and the US were applied to analyze the phenological periods of crops. The crop calendar of the US was similar to Northeast China. The cropland data included the GlobeLand30 dataset and Cultivated Layer data, which were employed to obtain the cropland of Northeast China and four US states, respectively. The overall accuracy of the GlobeLand30 dataset in 2010 was about 80% (Chen et al., 2015). Table S2 provides links to download datasets applied in this study.

3. Methods

3.1. Sentinel-2A/B image processing

The Sentinel-2 images were processed on the GEE platform. This study referred to the data processing process of Qiu et al (Qiu et al., 2021). Three spectral indices were calculated, including Optimized Soil Adjusted Vegetation Index (OSAVI) (equation (1)) (Rondeaux et al., 1996), Transformed Chlorophyll Absorption in Reflectance Index (TCARI) (equation (3)) (Haboudane et al., 2002) and Shortwave Infrared Water Stress Index (SIWSI) (equation (2)) (Fensholt and Sandholt, 2003). The OSAVI was employed to reflect vegetation growth dynamics and minimized the influences of soil background (Rondeaux et al., 1996). The TCARI/OSAVI could accurately predict crop chlorophyll content and was not affected by background reflectance properties (Haboudane et al., 2002). TCARI/OSAVI has a non-linear relationship with the chlorophyll content. The SIWSI could reflect soil moisture variations and canopy water stress better than the vegetation indices in the short term (Olsen et al., 2015). It is negatively related to the canopy water content (Fensholt and Sandholt, 2003).

$$OSAVI = \frac{1.16*(\rho_{NIR} - \rho_{Red})}{(\rho_{NIR} + \rho_{Red} + 0.16)} \quad (1)$$

$$\mathrm{TCARI} = 3 \times ((\rho_{VRE1} - \rho_{Red}) - 0.2 \times (\rho_{VRE1} - \rho_{Green}) \times \rho_{VRE1}/\rho_{Red}) \quad (2)$$

$$SIWSI = \frac{\rho_{SWIR1} - \rho_{NIR}}{\rho_{SWIR1} + \rho_{NIR}} \quad (3)$$

where ρ_{NIR},ρ_{Red},ρ_{Green},ρ_{VRE1} and ρ_{SWIR1} represented the reflectance of the Near-infrared (785–899 nm), Red (650–680 nm), Green (543–578 nm), Vegetation Red Edge1 (VRE1, 698–713 nm), and Short Wave Infrared band1 (SWIR1, 1,565–1,655 nm), respectively.

3.2. Designing phenology-based algorithm for soybean mapping

3.2.1. Extracting senescence water loss indicator and chlorophyll indicator

The phenological stages were extracted based on OSAVI temporal profiles. The heading date of the agricultural growth cycle was identified based on the annual maximum OSAVI. The heading date divided the whole growth period into the early growth stages and the late growth stages. The period of 50 days before and after the heading date was determined as the early and the late growth stages, respectively.

The dynamic pattern of SIWSI was opposite to that of OSAVI during the crop growing season due to its negative relationship with moisture concentration. There were significant differences in OSAVI and SIWSI temporal profiles during the late growth period (Fig. 2(a)). Compared with other crops such as maize and paddy rice, soybean is characterized by its distinguishable high senescence water loss: the canopy water content is only around 15% during the harvesting season. But, potato, peanut, sunflower, cotton, and soybean have similar senescence water loss. Potato and peanut mature earlier than soybean. Crop fields become bare soil with lower moisture concentrations than dry crops when crops mature. Most cotton and sunflower leaves fall off at maturity, resulting in high senescence water loss. Therefore, the variations of SIWSI temporal profiles of soybean were more distinctive than paddy rice, maize, sorghum, spring wheat, and canola (Fig. 2(a)). Additionally, soybean's distinctive senescence water loss is generally accompanied by rapid declines in photosynthesis activities reflected by the vegetation index (OSAVI). Therefore, the first phenology-based indicator, the ratio of

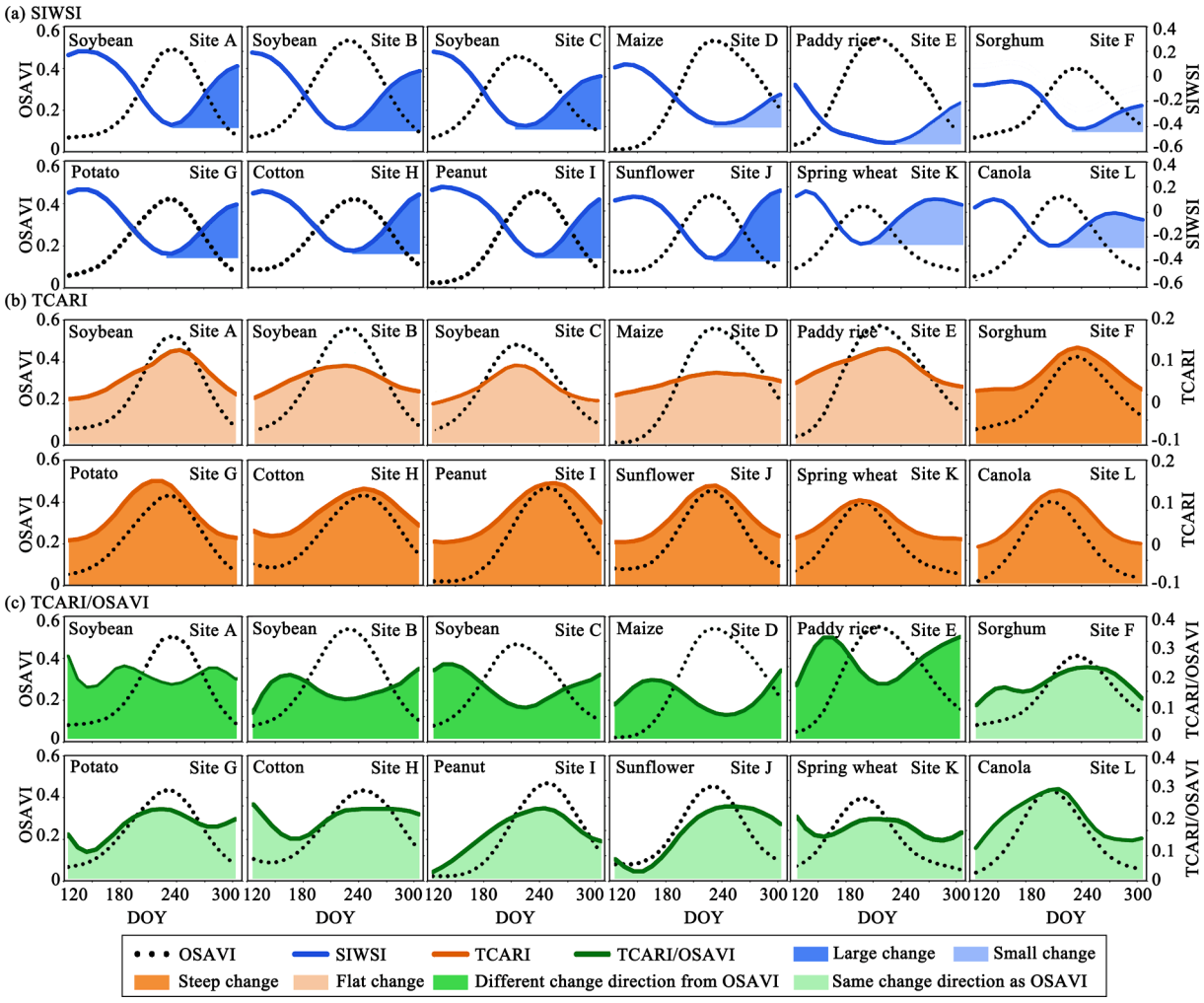

Fig. 2. Temporal profiles of (a) OSAVI, SIWSI, (b) TCARI and, (c) TCARI/OSAVI of soybean and other crops (Site A: 125°3′35″E, 43°4724 N; Site B: 128°19′48″E, 43°23′24″N; Site C: 128°25′12″E, 43°28′12″N; Site D: 125°55′12″E, 42°52′12″N; Site E: 128°27′36″E, 43°25′48″N; Site F: 123°47′24″E, 43°36′55″N; Site G: 125°44′24″E, 43°18′5″N; Site H: 88°19′48″W,33°0′36″N; Site I: 101°48′36″W,44°30′36″N; Site J: 100°27′3″W,46°27′36″N; Site K: 102°10′12″W,48°39′36″N; Site L: 99°50′24″ W,48°16′48″N).

change magnitudes of OSAVI to SIWSI (T1), was developed based on senescence water loss (Fig. 3(a)).

OSAVI followed the change of chlorophyll content, while the TCARI temporal profile of crops with higher chlorophyll content was flatter (Haboudane et al., 2002) (Fig. 2(b)). Therefore, crops with high chlorophyll content had lower TCARI/OSAVI values, and their dynamic pattern was opposite to OSAVI. But it was opposite when the chlorophyll content was low. These crops are divided into three groups based on the average chlorophyll content during the growth period. Maize has the highest chlorophyll content. Soybean, paddy rice, and sorghum have medium chlorophyll levels. Crops with short growth periods (i.e., soybean, potato, peanut, and spring wheat) (Fig. S1) and the unique canopy (i.e., canola, sunflower, and cotton) result in low chlorophyll content during the whole growth period. Therefore, the TCARI/OSAVI values of soybean were significantly higher than maize (Fig. 2(c)). The second phenology-based indicator, the mean concentration of TCARI/OSAVI during the whole growth period (T2), was developed based on the chlorophyll content (Fig. 3(b)). In addition, the TCARI/OSAVI temporal profile of soybean was opposite to peanut, potato, cotton, and sunflower (Fig. 2(c)). Therefore, the third phenology-based indicator, the accumulated variations of chlorophyll before and after the heading date (T3), was designed based on the temporal variations of chlorophyll content during the growth stages (Fig. 3(b)). The functions of these three indices based on OSAVI, SIWSI, and TCARI/OSAVI were provided as follows.

$$T1 = \frac{1 - (OSAVI_{Max} - OSAVI_{Min})}{1 + (SIWSI_{Max} - SIWSI_{Min})} \quad (4)$$

$$T2 = \overline{(TCARI/OSAVI)}_{Whole} \quad (5)$$

$$T3 = \sum_{i=start}^{End} ((TCARI/OSAVI)_{Heading} - (TCARI/OSAVI)_i) \quad (6)$$

where $OSAVI_{max}$ and $OSAVI_{min}$ represented the maximum and minimum values of OSAVI, $SIWSI_{max}$ and $SIWSI_{min}$ represented the maximum and minimum SIWSI values during the late growth stages. $\overline{(TCARI/OSAVI)}_{Whole}$ indicated the mean value of TCARI/OSAVI during the whole growth period;$(TCARI/OSAVI)_{Heading}$, and $(TCARI/OSAVI)_i$ represented TCARI/OSAVI during the heading date and date i, respectively; Start and end in the Σ denoted the start and end dates of the growth stages, respectively.

3.2.2. Developing soybean mapping algorithm

This study established a simple decision rule to distinguish soybean (Fig. 4). T1 was utilized to separate soybean from maize, paddy rice, sorghum, canola, and spring wheat. However, this indicator could not distinguish soybean from cotton, sunflower, peanut, potato, and a tiny amount of maize. T2 enhanced the separation between soybean and

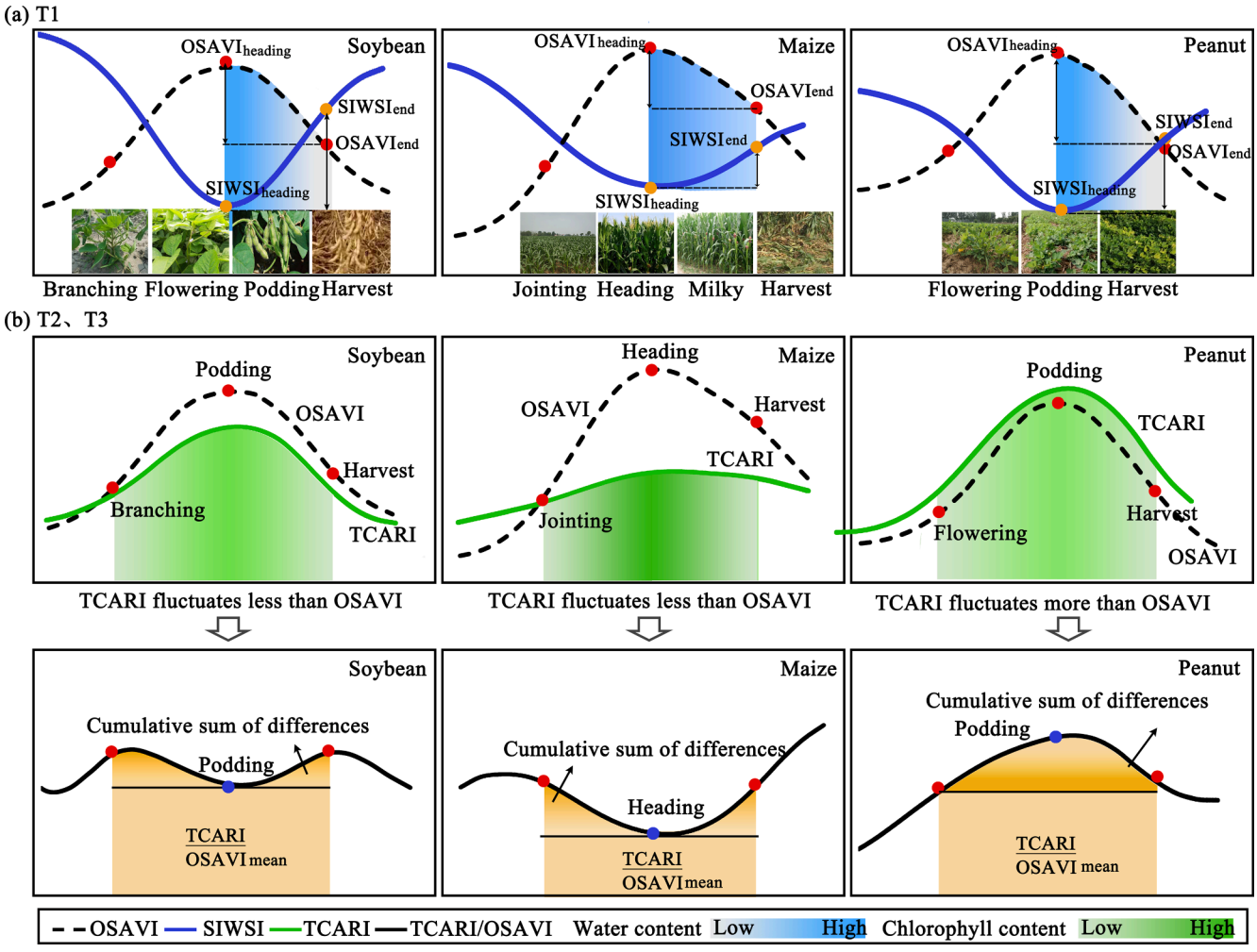

Fig. 3. Knowledge-based features and their interpretation.

maize. Furthermore, T3 was applied to distinguish soybean from cotton, sunflower, peanut, and potato. For soybean, the values of T1 and T3 are lower, and the value of T2 is higher. Therefore, a simple decision rule was established to distinguish soybean from non-soybean based on the proposed three phenology-based indices.

$$if(\mathrm{T1} < = \theta_1)and(\mathrm{T2} > = \theta_2)and(T3 <= \theta_3),\ Soybean = 1; else\ Soybean = 0 \quad (7)$$

where θ_1, θ_2 and θ_3 are constant. This algorithm was utilized in Northeast China and four US states. Land use/cover data was applied to obtain cultivated areas before classification.

3.3. Accuracy assessment of spatial distribution maps of soybean

Classification accuracy was evaluated by applying the agricultural statistics data and reference data. Sentinel-2- estimated soybean planting areas in Northeastern China and four U.S. states were aggregated to the municipal and county levels and compared with the corresponding agricultural statistical data. The spatial consistency of Sentinel-2- derived soybean map was evaluated by 5702 randomly selected reference points, including 1,702 sites in Northeast China and 4,000 sites in four US states. The confusion matrix was calculated by these reference sites. The classification accuracy of soybean was then assessed by using the producer's, user's, and overall accuracies from the confusion matrix.

4. Results

4.1. Soybean distribution maps in Northeast China and four US states

The thresholds for soybean mapping in Northeast China were determined by around 40% randomly selected reference points (1,135 sites) (Fig. 5(a)). The values of θ_1, θ_2, and θ_3 were 0.58, 0.16, and 0.05 in function (7). The proposed three phenology-based indices (T1, T2, and T3) distinguished soybean well from other crops. Most cropland pixels showed T1 values greater than 0.4, T2 values greater than 0, and T3 values less than 1.5 (Fig. 6(a)). The soybean distribution map in 2020 was obtained by the PSCC algorithm (Fig. 7(d)).

The PSCC algorithm and these three thresholds were further applied to Northeast China for other years and four US states. All Sentinel-2 derived soybean maps were displayed in Fig. 7, with a spatial resolution of 20 m. The soybean planting area in Northeast China from 2017 to 2021 was mainly distributed in Heilongjiang Province. The classification accuracy was lower than in Northeast China due to higher omission error when using these three thresholds in four US states (Fig. 5(b)). Therefore, these thresholds were redefined by 20% randomly selected reference points (1,000 sites). The values of θ_1, θ_2, and θ_3 were 0.59, 0.14, and 0, respectively. These three phenology-based indices provided an excellent distinction between soybean and non-soybean in four US states (Fig. 6(b)). A reliable soybean map in four US states in 2020 was obtained using the PSCC algorithm (Fig. 7(f)).

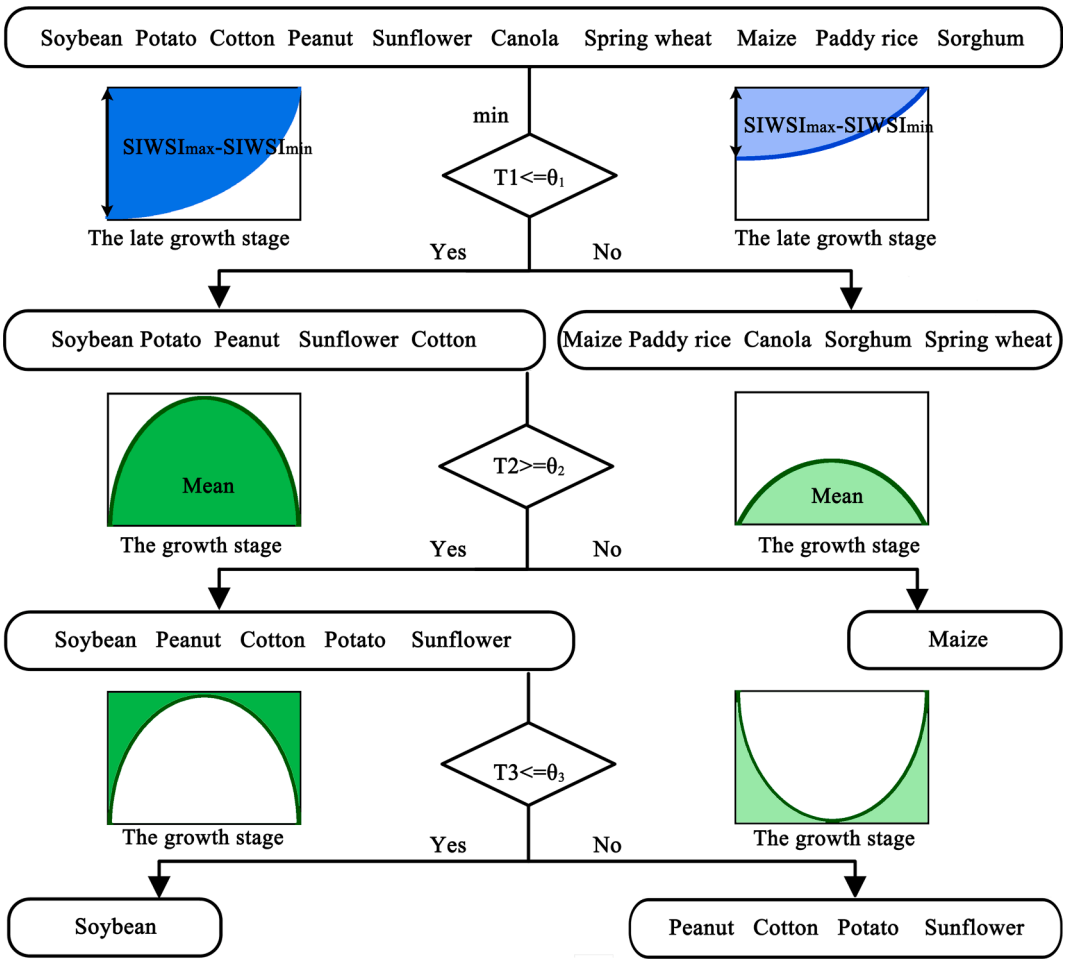

Fig. 4. Process of soybean classification based on three indices. Note that T1 cannot completely distinguish soybean from maize.

4.2. Accuracy assessment of soybean maps

Soybean planting area estimated by PSCC method was compared with agricultural statistical data in Northeast China and four US states. Soybean planting areas of Northeast China were 43,840 km^2 in 2017, 42,127 km^2 in 2018, and 45,949 km^2 in 2019, respectively. Compared with statistical data (40,300 km^2 in 2017, 39,204 km^2 in 2018, and 47,064 km^2 in 2019), the soybean planting area was overestimated by 8.78% and 7.46% in 2017 and 2018, respectively, but slightly underestimated by 2.37% in 2019. Soybean planting areas of Northeast China were gathered to the municipal level. Most municipalities showed good consistency with the statistical data, and R^2 reached above 0.83 (Fig. 8 (a), (b), and (c))). The soybean planting area of four US states in 2020 was 107,259 km^2, which was slightly underestimated (1,511 km^2) compared with statistical data. The soybean planting area of four US states agreed well with the statistical area at the county level, and R^2 was 0.8839 (Fig. 8, (d)). The underestimation of soybean planting area has occurred in some areas with less than 50% good quality observations (no cirrus clouds and opaque clouds), such as Mudanjiang in Northeast China and Vermilion, Champaign, Douglas, and Piatt in Illinois.

The spatial consistency of the Sentinel-2-estimated soybean map was evaluated with 5,702 reference points (Table 1). The overall accuracy of soybean maps using the T1 indicator was 75.92%, with a kappa coefficient of 0.5335 (Table S3). This indicator had a poor ability to distinguish soybean from maize, peanut, potato, sunflower and cotton. About 28% of maize was misclassified as soybean. The combination of T1 and T2 significantly improved the separation of soybean and maize, and the commission error for maize was reduced by 21.55%. The commission errors for peanut, potato, sunflower, and cotton were decreased when combining T1 and T3 indices. Furthermore, the combination of T1, T2 and T3 significantly improved the classification accuracy. For the 2,297 soybean sites, 2,085 sites were correctly classified (90.77% agreement). For the 3,405 non-soybean sites, 3,160 sites were accurately identified (92.80% agreement). And other 245 non-soybean sites were mistakenly classified as soybean, including 122 maize sites, 23 paddy rice sites, 35 peanut sites, 20 potato sites, 3 sorghum sites, 18 sunflower sites, 1 spring wheat site, 22 cotton sites, and 1 canola site. The overall accuracy was 91.99%, and the kappa index was 0.8338. The overall accuracy improved by 16.07% compared to only using T1 indicator for soybean mapping (Table S3).

4.3. Soybean expansion in ever-planted regions from 2015 to 2020

Soybean expansion in Northeast China mainly occurred in ever-planted regions from 2015 to 2020. The soybean planting area in Northeast China decreased continuously from 47,688 km^2 in 2008 to 29,033 km^2 in 2015, but increased significantly to 54,900 km^2 in 2020 and then decreased to 47,365 km^2 in 2021. More than 80% of the soybean planting area in Northeast China was distributed in Heilongjiang Province, concentrated primarily on Qiqihar, Heihe, Jiamusi, Harbin, Suihua, and Mudanjiang. The soybean planting area significantly reduced by 39.12% (18,655 km^2) from 2008 to 2015 (Fig. 9(a)). However, the soybean planting area expanded significantly by 89.10% (25,867 km^2) from 2015 to 2020. The proportion of soybean planting area to the cultivated area increased from 12.25% to 16.81%. Soybean expansion was significant in Heilongjiang Province, accounting for

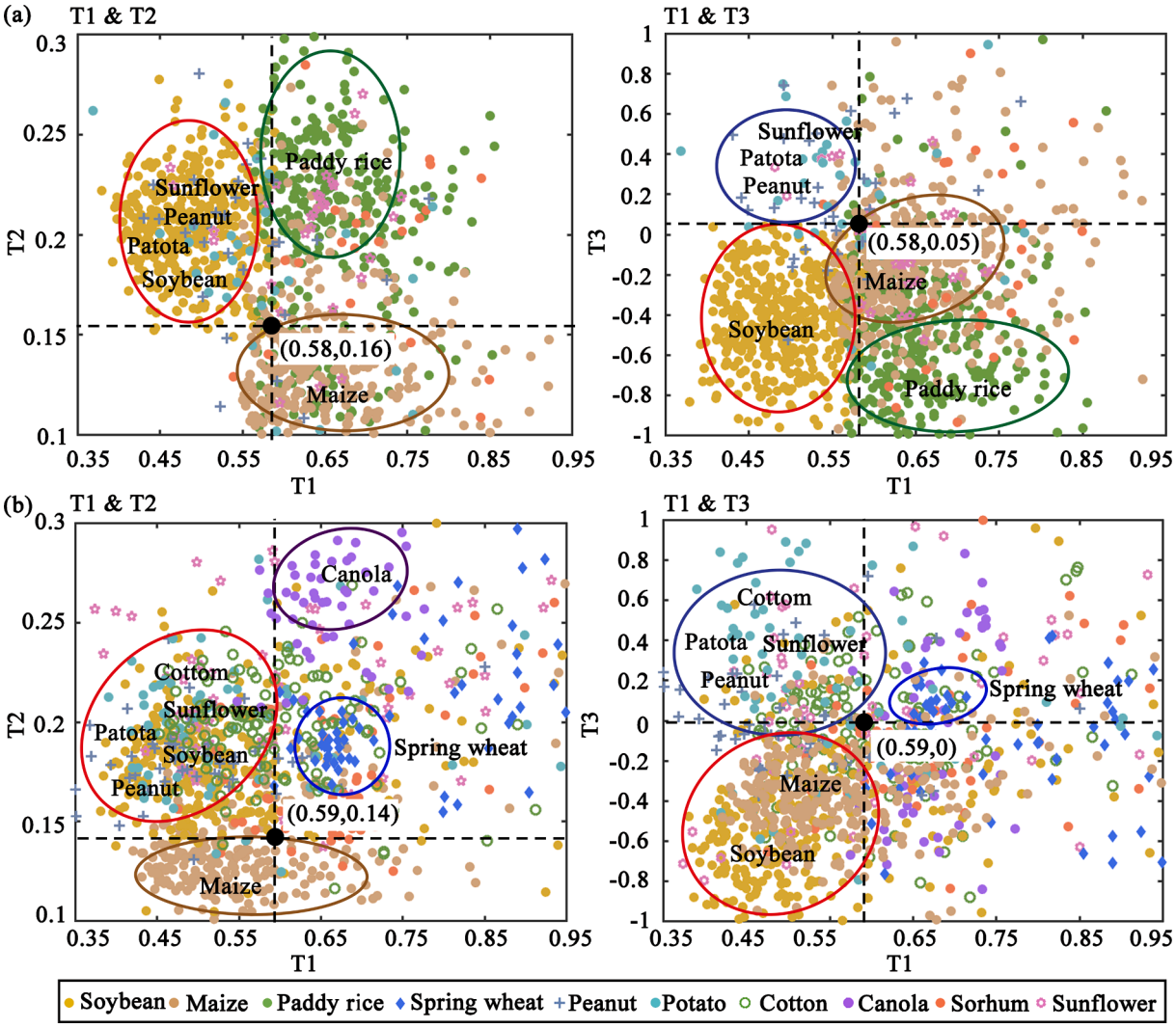

Fig. 5. Scatter plots of different crops within T1-T2 and T1-T3 in (a) Northeast China and (b) four US states.

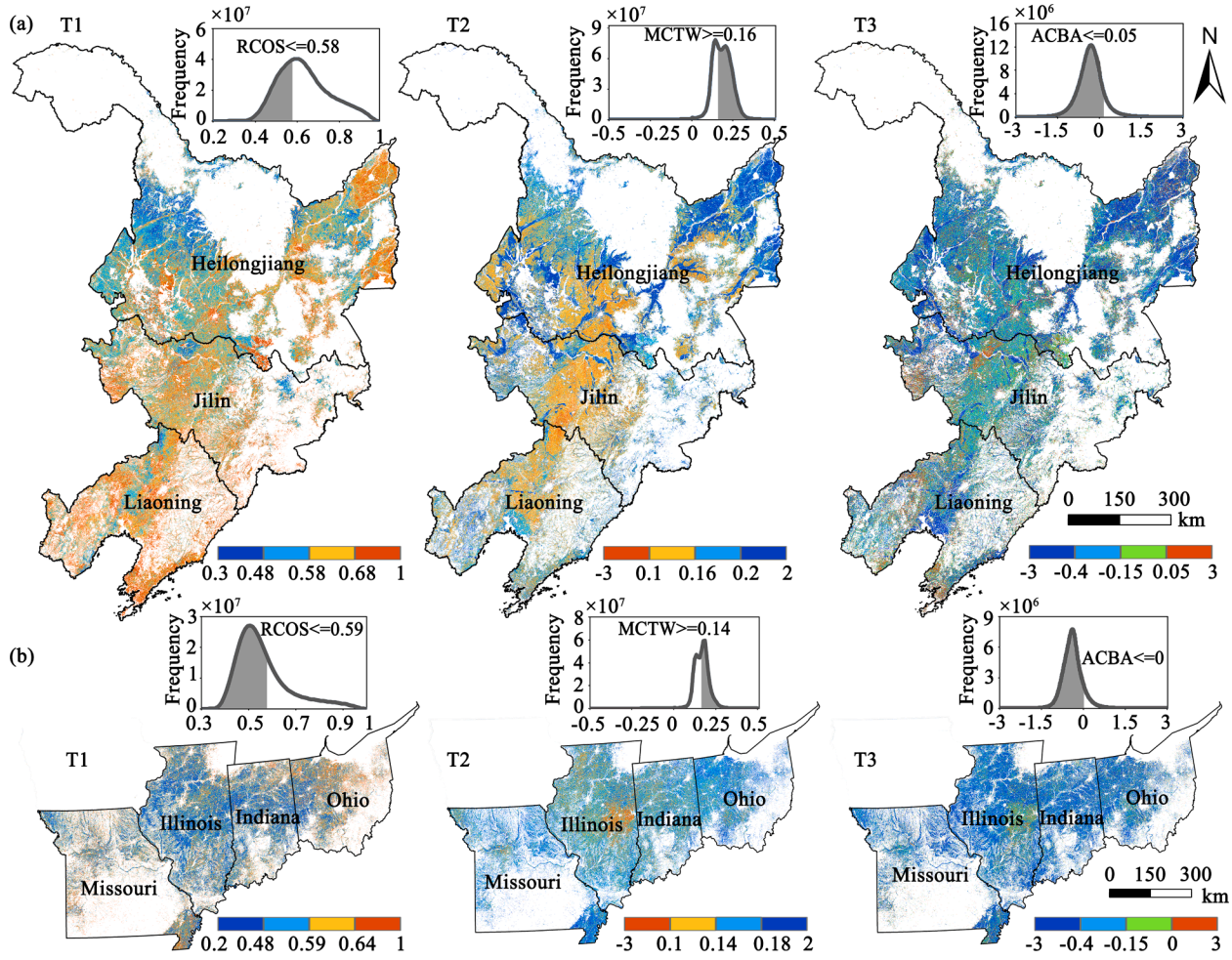

Fig. 6. Maps of T1, T2 and T3 indices in (a) Northeast China and (b) four US states in 2020.

about 68% (17,707 km^2) of the total expansion area (Fig. 9(b)). From 2020 to 2021, the soybean planting area showed a 13.73% (7,535 km^2) decrease, mainly in Heihe, Qiqihar, Suihua (Fig. 7(d) and (e))). There was a negative linear correlation between the changes in soybean planting area during 2015–2020 and during 2008–2015 ($R^2 = 0.3798$) (Fig. 9(c)). This showed that soybean expansion tended to be in ever-planted regions. Moreover, the primary soybean planting areas in Northeast China, such as Qiqihar, Heihe, Jiamusi, Harbin, Suihua, and Mudanjiang, have the most significant expansion trend.

5. Discussion

5.1. Advantages of the proposed PSCC method

This study developed a phenology-based automated soybean mapping method using water stress index and chlorophyll index temporal profiles. The advantages of the proposed PSCC method can be summarized in the following four points. First, The proposed PSCC method could be employed in other years and regions without retraining. This method has been validated in Northeast China from 2017 to 2021 and in four US states in 2020. Crop mapping in large regions is very economical and efficient without collecting reference data every year. When applied to a new region, the decision rule is still valid, but the threshold needs to adjust for higher classification accuracy slightly.

Second, chlorophyll content variation was better than canopy water content variation in distinguishing soybean and maize. Most current phenology-based soybean mapping methods mainly utilized the phenology parameters extracted by vegetation index (Zhong et al., 2014; Zhong et al., 2016b). However, it is difficult to separate crops with similar phenology, such as soybean, maize, and sorghum (Zhong et al., 2014). Spectral features are more reliable for distinguishing crops with similar phenology. This study distinguished soybean and sorghum with the ratio of the change magnitudes of OSAVI to SIWSI during the late growth stage (T1). However, the T1 indicator performed not well in distinguishing soybean from maize. A previous study also indicated that soybean and maize were not fully separable by differences in moisture content during the rapid-growing date (Zhong et al., 2016a). Recently, the pigment index (i.e., chlorophyll, anthocyanin, and carotenoid index) has received attention and performed well in highlighting crop growth (Qiu et al., 2021). Chlorophyll plays a decisive role in photosynthesis activities and is of great value in crop monitoring. To further separate soybean from maize, we explored the variations characteristics of chlorophyll content. The proposed T2 indicator, the mean concentration of TCARI/OSAVI during the whole growth period, significantly enhanced the separation of soybean and maize. The commission error of maize was reduced by about 22% (Table S4). The overall accuracy of soybean mapping was improved by 16.07% compared to simply applying canopy water content.

Third, the proposed T2 index has the potential to identify maize and canola. Although a recent study successfully used less variation in chlorophyll during the early growth stage to map peanut (Qiu et al., 2021), the chlorophyll levels of other crops have not yet been known. This study ranked ten crops based on the average chlorophyll content during the growth period, which provided opportunities for other crops mapping. Maize has low values of TCARI/OSAVI during the whole growth period due to the highest chlorophyll content. Therefore, the T2

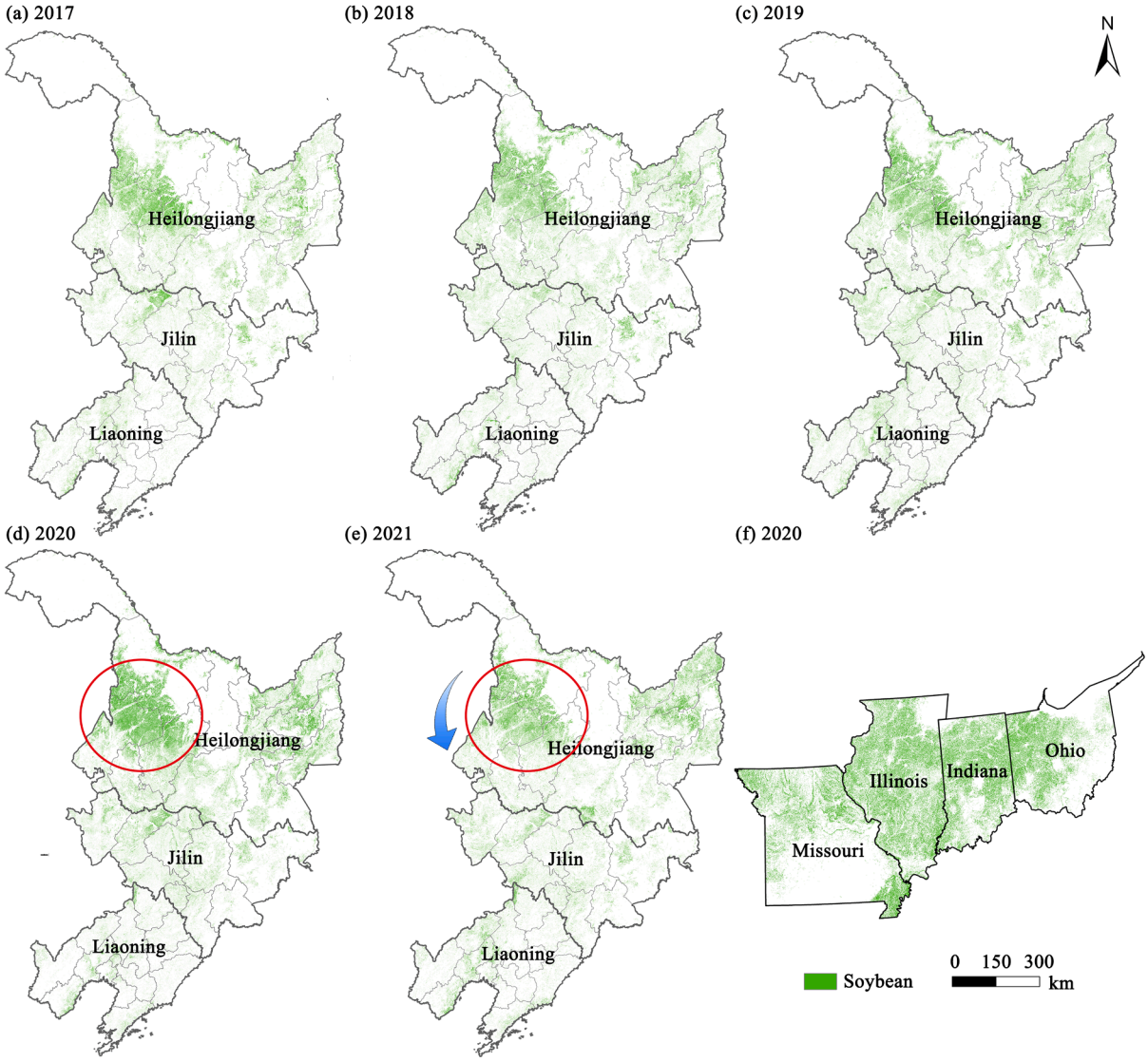

Fig. 7. Sentinel-2 derived soybean map in (a) to (e) Northeast China from 2017 to 2021 and (f) four US states in 2020.

indicator can effectively distinguish maize from other crops (Fig. 5). In addition, the mean concentration of TCARI/OSAVI of canola has a higher value than other crops due to lower chlorophyll content (Fig. 5). Therefore, the T2 indicator also can be applied to classify canola.

Fourth, this study provided a strategy for index-based methods for other crops mapping. The index-based crop mapping methods were simple and effective and have been used in staple crops (Qu et al., 2021; Xiao et al., 2005) and cash crops mapping (Ashourloo et al., 2020; Zhang et al., 2022). Index-based crop mapping algorithm has evolved from the subtraction-based method to the ratio-based method (Dong and Xiao, 2016). The ratio-based method performed better in coping with intra-class variation and was widely employed (Dong and Xiao, 2016). However, most methods utilized the change magnitudes of spectral indices at a particular phenological stage (da Silva Junior et al., 2020; Qiu et al., 2015; Qu et al., 2021). Using a large number of images resulted in better performance of the crop index (Ashourloo et al., 2019). This study utilized the temporal variations and mean concentration of chlorophyll index during the whole growth stage to design crop mapping indices, which were less disturbed by missing data (Fig. S2(b) and (c)). The temporal variations of multiple spectral indices may promote the development of index-based methods.

5.2. *Significances of soybean mapping*

A timely and reliable soybean map is essential to ensure food security and environmental sustainability. The soybean planting area in Northeast China has continually increased since 2015 and reached its peak in 2020. The goal of national soybean revitalization in 2020 is to reach 140 million mu of soybean planted area. Although the soybean planting area in Northeast China accounted for about half of the national soybean planting area, Northeast China contributed about 60% to the national goal of soybean revitalization. Soybean expansion in Northeast China is closely related to national agricultural policies (Liu et al., 2019). These policies provided substantial financial support for farmers to switch from maize to soybean (Liu et al., 2018). The soybean planting area expanded significantly in reclamation areas, such as Qiqihar, Heihe, Suihua, Jiamusi, Shuangya, and Harbi (Fig. 9(b)). The reclamation areas are state-owned enterprises and may respond more promptly to policies. However, the soybean planting area in Northeast China shows a declining trend in 2021. The Ministry of Agriculture and Rural Affairs (MARA) of China believes the main reason is the obvious benefits of planting maize. Some major producing areas have changed from soybean to maize.

Soybean production plans should be implemented in ever-planted

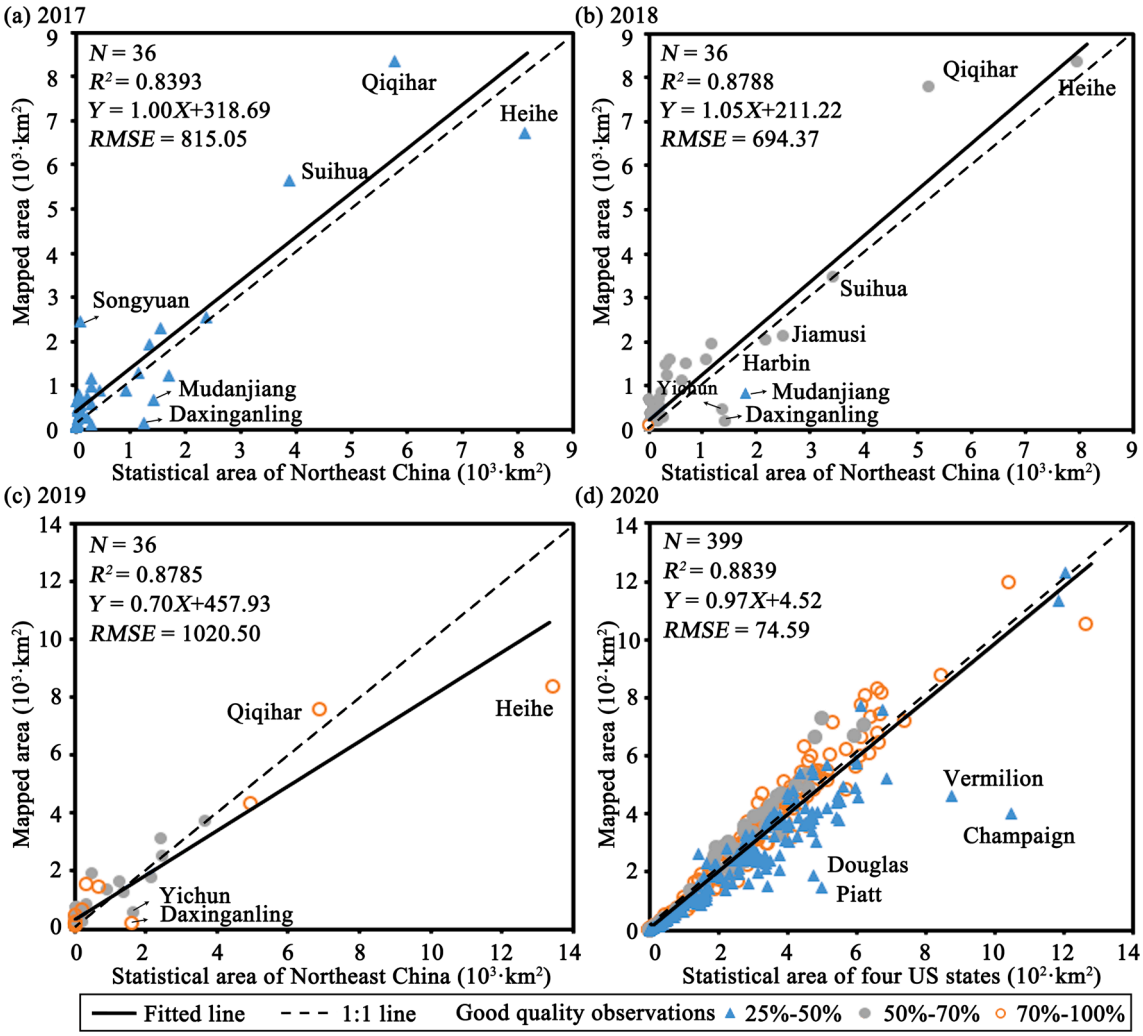

Fig. 8. The comparison of the Sentinel-2-estimated soybean planting areas with agricultural statistical data in (a) to (c) Northeast China from 2017 to 2019 and in (d) four US states in 2020.

areas. This study showed that soybean expansion occurred primarily in ever-planted regions, consistent with Yang et al (Yang et al., 2019). Currently, the stability of the global food supply is threatened by the severity of the Corona Virus Disease. To ensure food security, MARA has listed the soybean expansion as a significant task that must be completed in 2022. The key to expanding soybean production is increasing income. On the one hand, China should make great efforts to develop and promote new soybean varieties with high yield, high oil, and high protein. On the other hand, China should continue implementing the soybean rotation subsidy in ever-planted regions and increase the area of rotation subsidy. Crop rotation with soybean can increase yields and obtain additional environmental benefits due to the stimulation of the increase of rhizobia (Kumar et al., 2017; Scott et al., 2021).

5.3. Uncertainties and future works

The PSCC method has some disadvantages. This study determined the early and late growth stages dynamically based on the heading date. But, the lengths of the early and late growth stages were constant. Although the crop phenology in a specific area is relatively stable, the growth period in different regions may affect geographic conditions such as latitude, altitude, and temperature. The vegetation index reflecting crop phenology was often applied to extract key phenological periods to deal with phenology changes (Zhang et al., 2015; Zhong et al., 2016a). In addition, some studies have demonstrated that incorporating auxiliary data (such as agro-meteorological data and temperature conditions) is also an effective strategy for coping with the challenges introduced by changes in crop calendars (Qin et al., 2015; Zhang et al., 2014).

Table 1
Accuracy assessment of Sentinel-2-estimated soybean maps using reference data.

	Total	Soybean	Non - soybean	Producer accuracy (%)
Soybean	2297	2085	212	90.77
Non - soybean	3405	245	3160	92.80
User accuracy (%)		89.48	93.71	
Overall accuracy (%)	91.99			
Kappa	0.8338			

The PSCC method is suitable for regions with good-quality observations during the growth stage. When good quality observations are less due to cloud cover, the decrease in the change magnitudes of canopy water content could make soybean misclassified as other crops (Fig. S2 (a)). Soybean planting areas were often underestimated in counties with less than half of the excellent quality observations (Fig. 8). Multi-source data fusion can increase valid observation data during the growth period, such as MODIS, Landsat, and SAR data (Shi et al., 2022). However, MODIS and Landsat images lack red-edge bands for calculating the

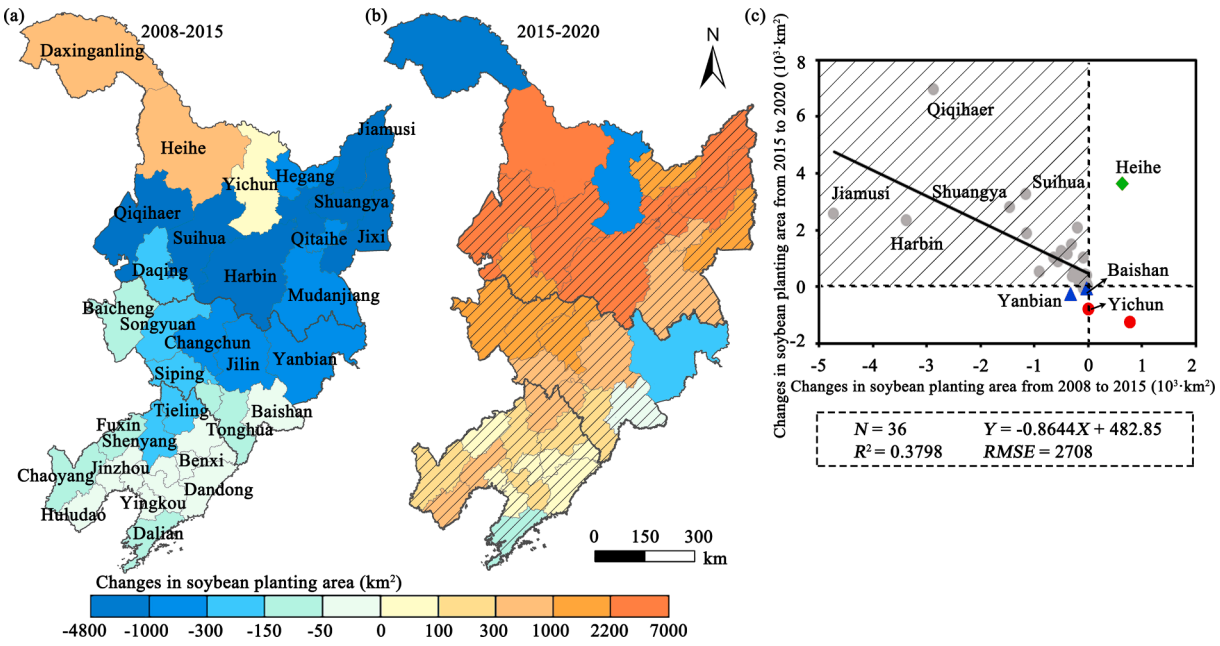

Fig. 9. Soybean change area at the municipal level in Northeast China during (a) 2008–2015 and (b) 2015–2020, and (c) relationship between soybean change area in Northeast China during 2008–2015 and 2015–2020. Note that the region with added texture represented that soybean planting area decreased in 2008–2015 but increased in 2015–2020, and soybean planting areas in 2008 and 2015 were from the provincial statistical yearbooks.

chlorophyll index. ENVISAT MERIS images have red-edge bands, and the soybean map with coarser spatial resolution could be obtained by fusion with Sentinel-2. However, the availability of optical data relies on weather conditions (Sudmanns et al., 2020). SAR data can monitor all-day and all-weather and the advantage of being free. The backscattering feature contains crop growth information (structure and canopy moisture) (Stankiewicz, 2006). A recent study has demonstrated that phenological indices derived from the Sentinel-1 time series can improve crop classification accuracy (Woźniak et al., 2022). Therefore, the combination of SAR and optical data has great potential for crop mapping.

6. Conclusions

This study developed a novel phenology-based algorithm for soybean mapping by exploring the variations characteristic of canopy water and chlorophyll content. The canopy water and chlorophyll content changed continuously with crop growth, which could indicate the physiological conditions of different crops. Soybean is characterized by high senescence water loss. Moreover, its chlorophyll content is lower than maize and higher than peanut, potato, cotton, and sunflower during the whole growth stage. Therefore, three phenology-based indices were designed for soybean mapping: the ratio of change magnitudes of OSAVI to SIWSI during the late growth stage (T1), the mean concentration of TCARI/OSAVI during the whole growth period (T2) and the accumulated variations of chlorophyll before and after heading date (T3). The proposed PSCC method was applied to Northeast China and four US states. The spatial distribution of soybean in Northeast China and four US states all showed good spatial agreement with reference data and correlation with agricultural statistics. This study revealed that the soybean planting area in Northeast China expanded continuously 25,867 km^2 from 2015 to 2020. Soybean expansion was mainly distributed in ever planted areas, especially the primary soybean planting areas. This study further disclosed that the soybean planting area decreased slightly 7,535 km^2 from 2020 to 2021 without updating official agricultural statistics data for 2021. This study was hoped to contribute to sustainable agricultural development by providing the spatial distribution data of soybean.

CRediT authorship contribution statement

Yingze Huang: Conceptualization, Methodology, Software, Visualization, Formal analysis, Writing – original draft. **Bingwen Qiu:** Project administration, Funding acquisition, Writing – review & editing. **Chongcheng Chen:** Writing – review & editing. **Xiaolin Zhu:** Writing – review & editing. **Wenbin Wu:** Writing – review & editing. **Fanchen Jiang:** Validation, Writing – review & editing. **Duoduo Lin:** Data curation, Writing – review & editing. **Yufeng Peng:** Writing – review & editing.

Declaration of Competing Interest

The authors declare that they have no known competing financial interests or personal relationships that could have appeared to influence the work reported in this paper.

Acknowledgements

This work was supported by the National Natural Science Foundation of China (grant no. 42171325, 41771468), funding from the Science Bureau of Fujian Province (2020N5002) and Fujian provincial department of ecology and environment (2022R023).

Appendix A. Supplementary data

Supplementary data to this article can be found online at https://doi.org/10.1016/j.jag.2022.102801.

References

Agomoh, I.V., Drury, C.F., Yang, X., Phillips, L.A., Reynolds, W.D., 2021. Crop rotation enhances soybean yields and soil health indicators. Soil Sci. Soc. Am. J. 85 (4), 1185–1195.

Ashourloo, D., Shahrabi, H.S., Azadbakht, M., Aghighi, H., Nematollahi, H., Alimohammadi, A., Matkan, A.A., 2019. Automatic canola mapping using time series of sentinel 2 images. ISPRS J. Photogramm. Remote Sens. 156, 63–76.

Ashourloo, D., Shahrabi, H.S., Azadbakht, M., Rad, A.M., Aghighi, H., Radiom, S., 2020. A novel method for automatic potato mapping using time series of Sentinel-2 images. Comput. Electron. Agric. 175, 1–13.

Boryan, C., Yang, Z., Mueller, R., Craig, M., 2011. Monitoring US agriculture: the US department of agriculture, national agricultural statistics service, cropland data layer program. Geocarto Int. 26 (5), 341–358.
Cai, Y., Guan, K., Peng, J., Wang, S., Seifert, C., Wardlow, B., Li, Z., 2018. A high-performance and in-season classification system of field-level crop types using time-series Landsat data and a machine learning approach. Remote Sens. Environ. 210, 35–47.
Chen, J., Chen, J., Liao, A., Cao, X., Chen, L., Chen, X., He, C., Han, G., Peng, S., Lu, M., Zhang, W., Tong, X., Mills, J., 2015. Global land cover mapping at 30 m resolution: A POK-based operational approach. ISPRS J. Photogramm. Remote Sens. 103, 7–27.
Silva, C.A., Nanni, M.R., Teodoro, P.E., Silva, G.F.C., 2017. Vegetation indices for discrimination of soybean areas: A new approach. Agron. J. 109 (4), 1331–1343.
da Silva Junior, C.A., Leonel-Junior, A.H.S., Rossi, F.S., Correia Filho, W.L.F., de Barros Santiago, D., de Oliveira-Júnior, J.F., Teodoro, P.E., Lima, M., Capristo-Silva, G.F., 2020. Mapping soybean planting area in midwest Brazil with remotely sensed images and phenology-based algorithm using the Google Earth Engine platform. Comput. Electron. Agric. 169, 1–10.
de Souza, C.H.W., Mercante, E., Johann, J.A., Lamparelli, R.A.C., Uribe-Opazo, M.A., 2015. Mapping and discrimination of soya bean and corn crops using spectro-temporal profiles of vegetation indices. Int. J. Remote Sens. 36 (7), 1809–1824.
Dong, J., Xiao, X., 2016. Evolution of regional to global paddy rice mapping methods: A review. ISPRS J. Photogramm. Remote Sens. 119, 214–227.
Esquerdo, J.C.D.M., Zullo Júnior, J., Antunes, J.F.G., 2011. Use of NDVI/AVHRR time-series profiles for soybean crop monitoring in Brazil. Int. J. Remote Sens. 32 (13), 3711–3727.
Fensholt, R., Sandholt, I., 2003. Derivation of a shortwave infrared water stress index from MODIS near- and shortwave infrared data in a semiarid environment. Remote Sens. Environ. 87 (1), 111–121.
Haboudane, D., Miller, J.R., Tremblay, N., Zarco-Tejada, P.J., Dextraze, L., 2002. Integrated narrow-band vegetation indices for prediction of crop chlorophyll content for application to precision agriculture. Remote Sens. Environ. 81 (2-3), 416–426.
Jain, M., Mondal, P., Galford, G.L., Fiske, G., DeFries, R.S., 2017. An automated approach to map winter cropped area of smallholder farms across large scales using MODIS imagery. Remote Sens. 9, 1–13.
Jin, Z., Azzari, G., You, C., Di Tommaso, S., Aston, S., Burke, M., Lobell, D.B., 2019. Smallholder maize area and yield mapping at national scales with Google Earth Engine. Remote Sens. Environ. 228, 115–128.
Kumar, V., Rawat, A., Rao, D., 2017. Population ecology of soybean-rhizobia in diverse crop rotations in Central India. Agric. Ecosyst. Environ. 240, 261–268.
Liu, S., Zhang, P., Marley, B., Liu, W., 2019. The factors affecting farmers' soybean planting behavior in Heilongjiang Province, China. Agriculture 9, 1–13.
Liu, W., Dong, J., Xiang, K., Wang, S., Han, W., Yuan, W., 2018. A sub-pixel method for estimating planting fraction of paddy rice in Northeast China. Remote Sens. Environ. 205, 305–314.
Olsen, J.L., Stisen, S., Proud, S.R., Fensholt, R., 2015. Evaluating EO-based canopy water stress from seasonally detrended NDVI and SIWSI with modeled evapotranspiration in the Senegal River Basin. Remote Sens. Environ. 159, 57–69.
Peña, M., Brenning, A., 2015. Assessing fruit-tree crop classification from Landsat-8 time series for the Maipo Valley, Chile. Remote Sens. Environ. 171, 234–244.
Qin, Y., Xiao, X., Dong, J., Zhou, Y., Zhu, Z., Zhang, G., Du, G., Jin, C., Kou, W., Wang, J., Li, X., 2015. Mapping paddy rice planting area in cold temperate climate region through analysis of time series Landsat 8 (OLI), Landsat 7 (ETM+) and MODIS imagery. ISPRS J. Photogramm. Remote Sens. 105, 220–233.
Qiu, B., Huang, Y., Chen, C., Tang, Z., Zou, F., 2018. Mapping spatiotemporal dynamics of maize in China from 2005 to 2017 through designing leaf moisture based indicator from Normalized Multi-band Drought Index. Comput. Electron. Agric. 153, 82–93.
Qiu, B., Jiang, F., Chen, C., Tang, Z., Wu, W., Berry, J., 2021. Phenology-pigment based automated peanut mapping using sentinel-2 images. GIScience & Remote Sensing 58 (8), 1335–1351.
Qiu, B., Li, W., Tang, Z., Chen, C., Qi, W., 2015. Mapping paddy rice areas based on vegetation phenology and surface moisture conditions. Ecol. Ind. 56, 79–86.
Qiu, B., Lu, D., Tang, Z., Song, D., Zeng, Y., Wang, Z., Chen, C., Chen, N., Huang, H., Xu, W., 2017a. Mapping cropping intensity trends in China during 1982–2013. Appl. Geogr. 79, 212–222.
Qiu, B., Luo, Y., Tang, Z., Chen, C., Lu, D., Huang, H., Chen, Y., Chen, N., Xu, W., 2017b. Winter wheat mapping combining variations before and after estimated heading dates. ISPRS J. Photogramm. Remote Sens. 123, 35–46.
Qu, C., Li, P., Zhang, C., 2021. A spectral index for winter wheat mapping using multi-temporal Landsat NDVI data of key growth stages. ISPRS J. Photogramm. Remote Sens. 175, 431–447.
Rębilas, K., Klimek-Kopyra, A., Bacior, M., Zając, T., 2020. A model for the yield losses estimation in an early soybean (Glycine max (L.) Merr.) cultivar depending on the cutting height at harvest. Field Crops Res. 254, 1–10.
Ren, T., Xu, H., Cai, X., Yu, S., Qi, J., 2022. Smallholder Crop Type Mapping and Rotation Monitoring in Mountainous Areas with Sentinel-1/2 Imagery. Remote Sens. 14, 1–18.
Rondeaux, G., Steven, M., Baret, F., 1996. Optimization of soil-adjusted vegetation indices. Remote Sens. Environ. 55 (2), 95–107.
Scott, D.A., Eberle, C., Gesch, R.W., Schneider, S., Weyers, S., Johnson, J.M., 2021. Yield, nitrogen, and water use benefits of diversifying crop rotations with specialty oilseeds. Agric. Ecosyst. Environ. 317, 1–10.
Sharifi, A., 2020. Remotely sensed vegetation indices for crop nutrition mapping. J. Sci. Food Agric. 100 (14), 5191–5196.
Shi, W., Guo, D., Zhang, H., 2022. A reliable and adaptive spatiotemporal data fusion method for blending multi-spatiotemporal-resolution satellite images. Remote Sens. Environ. 268, 1–24.
Song, X.-P., Potapov, P.V., Krylov, A., King, L., Di Bella, C.M., Hudson, A., Khan, A., Adusei, B., Stehman, S.V., Hansen, M.C., 2017. National-scale soybean mapping and area estimation in the United States using medium resolution satellite imagery and field survey. Remote Sens. Environ. 190, 383–395.
Stankiewicz, K.A., 2006. The efficiency of crop recognition on ENVISAT ASAR images in two growing seasons. IEEE Trans. Geosci. Remote Sens. 44 (4), 806–814.
Sudmanns, M., Tiede, D., Augustin, H., Lang, S., 2020. Assessing global Sentinel-2 coverage dynamics and data availability for operational Earth observation (EO) applications using the EO-Compass. Int. J. Digital Earth 13 (7), 768–784.
Thenkabail, P.S., Biradar, C.M., Noojipady, P., Dheeravath, V., Li, Y., Velpuri, M., Gumma, M., Gangalakunta, O.R.P., Turral, H., Cai, X., Vithanage, J., Schull, M.A., Dutta, R., 2009. Global irrigated area map (GIAM), derived from remote sensing, for the end of the last millennium. Int. J. Remote Sens. 30 (14), 3679–3733.
Tian, H., Chen, T., Li, Q., Mei, Q., Wang, S., Yang, M., Wang, Y., Qin, Y., 2022. A Novel Spectral Index for Automatic Canola Mapping by Using Sentinel-2 Imagery. Remote Sens. 14, 1–18.
Tran, K.H., Zhang, H.K., McMaine, J.T., Zhang, X., Luo, D., 2022. 10 m crop type mapping using Sentinel-2 reflectance and 30 m cropland data layer product. Int. J. Appl. Earth Obs. Geoinf. 107, 1–16.
Waldner, F., Canto, G.S., Defourny, P., 2015. Automated annual cropland mapping using knowledge-based temporal features. ISPRS J. Photogramm. Remote Sens. 110, 1–13.
Wang, J., Xiao, X., Liu, L., Wu, X., Qin, Y., Steiner, J.L., Dong, J., 2020. Mapping sugarcane plantation dynamics in Guangxi, China, by time series Sentinel-1, Sentinel-2 and Landsat images. Remote Sens. Environ. 247, 1–16.
Wang, N., Zhai, Y., Zhang, L., 2021. Automatic Cotton Mapping Using Time Series of Sentinel-2 Images. Remote Sens. 13, 1–19.
Wang, S., Azzari, G., Lobell, D.B., 2019. Crop type mapping without field-level labels: Random forest transfer and unsupervised clustering techniques. Remote Sens. Environ. 222, 303–317.
Weiss, M., Jacob, F., Duveiller, G., 2020. Remote sensing for agricultural applications: A meta-review. Remote Sens. Environ. 236, 1–19.
Wong, C.Y., D'Odorico, P., Bhathena, Y., Arain, M.A., Ensminger, I., 2019. Carotenoid based vegetation indices for accurate monitoring of the phenology of photosynthesis at the leaf-scale in deciduous and evergreen trees. Remote Sens. Environ. 233, 1–14.
Woźniak, E., Rybicki, M., Kofman, W., Aleksandrowicz, S., Wojtkowski, C., Lewiński, S., Bojanowski, J., Musiał, J., Milewski, T., Slesiński, P., Łączyński, A., 2022. Multi-temporal phenological indices derived from time series Sentinel-1 images to country-wide crop classification. Int. J. Appl. Earth Obs. Geoinf. 107, 102683.
Xiao, X., Boles, S., Liu, J., Zhuang, D., Frolking, S., Li, C., Salas, W., Moore, B., 2005. Mapping paddy rice agriculture in southern China using multi-temporal MODIS images. Remote Sens. Environ. 95 (4), 480–492.
Xu, J., Yang, J., Xiong, X., Li, H., Huang, J., Ting, K., Ying, Y., Lin, T., 2021. Towards interpreting multi-temporal deep learning models in crop mapping. Remote Sens. Environ. 264, 1–21.
Xun, L., Zhang, J., Cao, D., Yang, S., Yao, F., 2021. A novel cotton mapping index combining Sentinel-1 SAR and Sentinel-2 multispectral imagery. ISPRS J. Photogramm. Remote Sens. 181, 148–166.
Yang, L., Wang, L., Huang, J., Mansaray, L.R., Mijiti, R., 2019. Monitoring policy-driven crop area adjustments in northeast China using Landsat-8 imagery. Int. J. Appl. Earth Obs. Geoinf. 82, 1–18.
You, N., Dong, J., Huang, J., Du, G., Zhang, G., He, Y., Yang, T., Di, Y., Xiao, X., 2021. The 10-m crop type maps in Northeast China during 2017–2019. Sci. Data 8, 1–11.
Zang, Y., Chen, X., Chen, J., Tian, Y., Shi, Y., Cao, X., Cui, X., 2020. Remote Sensing Index for Mapping Canola Flowers Using MODIS Data. Remote Sens. 12, 1–19.
Zhang, G., Xiao, X., Dong, J., Kou, W., Jin, C., Qin, Y., Zhou, Y., Wang, J., Menarguez, M. A., Biradar, C., 2015. Mapping paddy rice planting areas through time series analysis of MODIS land surface temperature and vegetation index data. ISPRS J. Photogramm. Remote Sens. 106, 157–171.
Zhang, H., Kang, J., Xu, X., Zhang, L., 2020. Accessing the temporal and spectral features in crop type mapping using multi-temporal Sentinel-2 imagery: A case study of Yi'an County, Heilongjiang province, China. Comput. Electron. Agric. 176, 1–15.
Zhang, H., Liu, W., Zhang, L., 2022. Seamless and automated rapeseed mapping for large cloudy regions using time-series optical satellite imagery. ISPRS J. Photogramm. Remote Sens. 184, 45–62.
Zhang, J., Feng, L., Yao, F., 2014. Improved maize cultivated area estimation over a large scale combining MODIS–EVI time series data and crop phenological information. ISPRS J. Photogramm. Remote Sens. 94, 102–113.
Zheng, B., Myint, S.W., Thenkabail, P.S., Aggarwal, R.M., 2015. A support vector machine to identify irrigated crop types using time-series Landsat NDVI data. Int. J. Appl. Earth Obs. Geoinf. 34, 103–112.
Zhong, L., Gong, P., Biging, G.S., 2014. Efficient corn and soybean mapping with temporal extendability: A multi-year experiment using Landsat imagery. Remote Sens. Environ. 140, 1–13.
Zhong, L., Hawkins, T., Biging, G., Gong, P., 2011. A phenology-based approach to map crop types in the San Joaquin Valley, California. Int. J. Remote Sens. 32 (22), 7777–7804.
Zhong, L., Hu, L., Yu, L., Gong, P., Biging, G.S., 2016a. Automated mapping of soybean and corn using phenology. ISPRS J. Photogramm. Remote Sens. 119, 151–164.
Zhong, L., Yu, L., Li, X., Hu, L., Gong, P., 2016b. Rapid corn and soybean mapping in US Corn Belt and neighboring areas. Sci. Rep. 6, 1–14.